Geochemistry Geophysics Geosystems G3

Article
Volume 13, Number 1
31 May 2012
Q0AF04, doi:10.1029/2011GC003891
ISSN: 1525-2027

Published by AGU and the Geochemical Society

Hydrothermal activity in the Northwest Lau Backarc Basin: Evidence from water column measurements

J. E. Lupton
NOAA Pacific Marine Environmental Laboratory, Newport, Oregon 97365, USA (john.e.lupton@noaa.gov)

R. J. Arculus
Research School of Earth Sciences, Australian National University, Canberra, ACT 0200, Australia

J. Resing
NOAA Pacific Marine Environmental Laboratory, Seattle, Washington 98195, USA

G. J. Massoth
Mass-Ex3 Consulting, Renton, Washington 98056, USA

R. R. Greene and L. J. Evans
Cooperative Institute of Marine Resources Studies, Oregon State University, Newport, Oregon 97365, USA

N. Buck
NOAA Pacific Marine Environmental Laboratory, Seattle, Washington 98195, USA

[1] The Northwest Lau Backarc Basin, consisting of the Northwest Lau Spreading Center (NWLSC) and the Rochambeau Rifts (RR), is unique in having elevated $^3He/^4He$ ratios (up to 28 R_a) in the erupted lavas, clearly indicating a hot spot or ocean island basalt (OIB)-type signature. This OIB-type helium signature does not appear in any other part of the Lau Basin. Water column plume surveys conducted in 2008 and 2010 identified several sites of active hydrothermal discharge along the NWLSC-RR and showed that the incidence of hydrothermal activity is high, consistent with the high spreading rate of ~100 mm/year. Hydrocasts into the Central Caldera and Southern Caldera of the NWLSC detected elevated $^3He/^4He$ (δ^3He = 55% and 100%, respectively), trace metals (TMn, TFe), and suspended particles, indicating localized hydrothermal venting at these two sites. Hydrocasts along the northern rift zone of the NWLSC also had excess δ^3He, TMn, and suspended particles suggesting additional sites of hydrothermal activity. The RR are dominated by Lobster Caldera, a large volcano with four radiating rift zones. Hydrocasts into Lobster Caldera in 2008 detected high δ^3He (up to 239%) and suspended particle and TMn signals, indicating active venting within the caldera. A repeat survey of Lobster in 2010 confirmed the site was still active two years later. Plumes at Lobster Caldera and Central Caldera have end-member $^3He/^4He$ ratios of 19 R_a and 11 R_a, respectively, confirming that hot spot-type helium is also present in the hydrothermal fluids.

Components: 9000 words, 12 figures.

Keywords: Lau Basin; back arc; helium; hydrothermal.

Index Terms: 1034 Geochemistry: Hydrothermal systems (0450, 3017, 3616, 4832, 8135, 8424); 8413 Volcanology: Subduction zone processes (1031, 3060, 3613, 8170); 8424 Volcanology: Hydrothermal systems (0450, 1034, 3017, 3616, 4832, 8135).

Received 6 October 2011; **Revised** 13 April 2012; **Accepted** 13 April 2012; **Published** 31 May 2012.

Lupton, J. E., R. J. Arculus, J. Resing, G. J. Massoth, R. R. Greene, L. J. Evans, and N. Buck (2012), Hydrothermal activity in the Northwest Lau Backarc Basin: Evidence from water column measurements, *Geochem. Geophys. Geosyst.*, *13*, Q0AF04, doi:10.1029/2011GC003891.

Theme: Assessing Magmatic, Neovolcanic, Hydrothermal, and Biological Processes along Intra-Oceanic Arcs and Back-Arcs

1. Introduction

[2] The northern Lau Basin is the Earth's fastest-opening backarc basin opening at ~160 mm/yr [*Bevis et al.*, 1995; *Pelletier et al.*, 1998; *Zellmer and Taylor*, 2001], with this extension almost evenly divided between the Northwest Lau Spreading Center (NWLSC) and the Northeast Lau Spreading Center (NELSC). The region experiences extremely rapid subduction along the Tofua Arc (~240 mm/yr) [*Zellmer and Taylor*, 2001], which is thought to result in rapid roll back and mantle inflow from the Samoan hot spot [*Wiens et al.*, 2006]. This combination of effects is thought to produce elevated mantle temperatures and vigorous mantle flow patterns in the Lau Basin. The rapid extension and elevated temperatures may result in enhanced magmatic and hydrothermal activity in the Lau Basin [*German et al.*, 2006; *Keller et al.*, 2008; *Embley et al.*, 2009; *Kim et al.*, 2009; *Baker et al.*, 2011; *Resing et al.*, 2011]. In this paper we examine whether the rapid extension accommodated by the NWLSC is expressed by elevated magmatic activity as identified by contemporaneous hydrothermal activity.

[3] The northern Lau Basin has several zones of active spreading [*Hawkins*, 1995; *Pelletier et al.*, 1998, 2001] (Figure 1). In the northeastern part of the Basin, closest to the Tofua Arc, the Fonualei Rift and Spreading Center (FRSC) steps westward and northward to the Mangatolu Triple Junction (MTJ) and Northeast Lau Spreading Center (NELSC). Farther west, the Northwest Lau Spreading Center (NWLSC) is another major extensional zone which terminates in the south against a long right-lateral transform fault known as the Peggy Ridge. At its western end, the Peggy Ridge terminates at the Futuna Spreading Center (FSC), while at its southeastern end it breaks into a series of short left-stepping rift-segments known as the Lau Extensional Transform Zone (LETZ) [*Martinez and Taylor*, 2006]. Northeast of the NWLSC is a complex series of rifts, pull-apart basins, and volcanic centers forming the Rochambeau Rifts (RR). The RR were previously known as the Niuafo'ou Spreading Center. However, multibeam mapping has shown there is no clear zone of spreading in this region. Since the Rifts are proximal to Rochambeau, a major submarine volcanic center, they have been renamed accordingly [*Arculus*, 2008]. *Pelletier et al.* [1998] estimated that the overall opening rate for the northern Lau Basin is about 159 mm/yr, while *Bird* [2003], using a digital plate model, estimated spreading rates for the RR, the NWLSC, and the NELSC at approximately 110, 75, and 120 mm/yr, respectively. Thus the northeastern and northwestern Lau spreading centers apparently each accommodate an opening rate of ~100 mm/yr.

[4] Helium isotopes have been shown to be a useful geochemical tracer for distinguishing between depleted mantle or mid-ocean ridge (MOR-type) and fertile (hot spot) mantle sources. In particular, mid-ocean ridge basalts (MORBs) have fairly uniform $^3He/^4He$ ratios, while oceanic hot spots typically have $^3He/^4He$ ratios either much higher or much lower than the MOR-type signature. The NWLSC–RR extensional zone has attracted considerable attention due to the unique isotopic signature of the erupted lavas in this region. For example, *Poreda and Craig* [1992] measured elevated $^3He/^4He$ in three samples from the RR (up to 22 R_a), providing an early indication of the presence of a hot spot component in this backarc extensional zone. In a more extensive study of the same area, *Lupton et al.* [2009] showed that a suite of 29 basalts dredged along the RR and NWLSC all had elevated $^3He/^4He$ (11 to 28 R_a), much higher than the ratio of 7 to 9 R_a typically observed in MORBs [*Graham*, 2002]. *Lupton et al.* [2009] demonstrated that these elevated helium isotope ratios are not confined to the RR, but extend southward along the NWLSC to the Peggy Ridge. In contrast to the NWLSC-RR, the spreading centers of the northeast Lau Basin have typical MOR-type helium isotope ratios [*Poreda and Craig*, 1992; *Hilton et al.*, 1993; *Honda et al.*, 1993; *Lupton et al.*, 2009]. Thus these

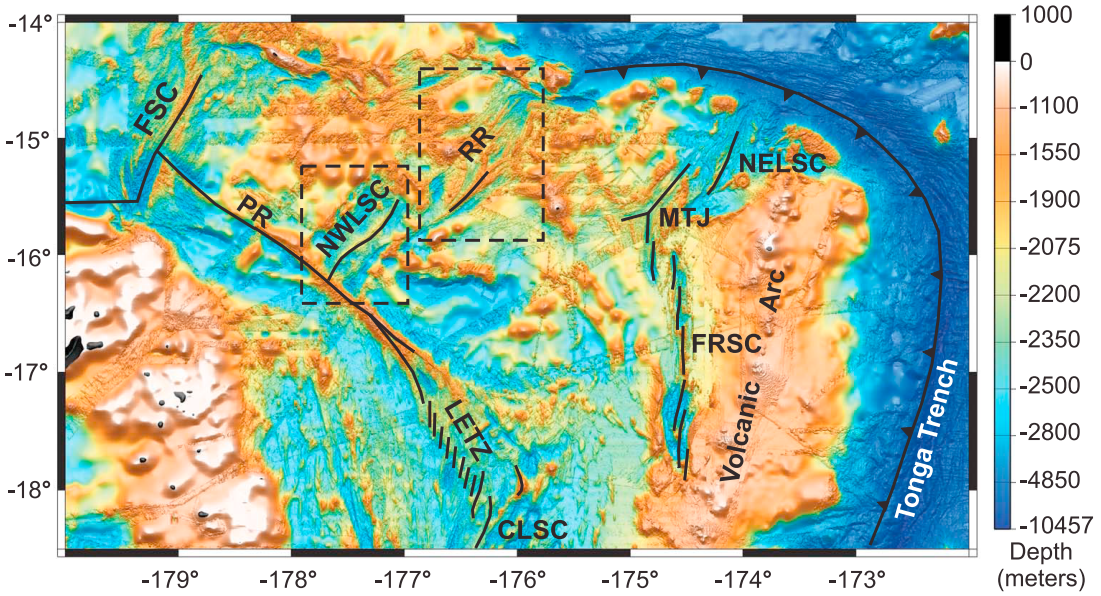

Figure 1. Relief map of the northern Lau Basin showing the major rift zones and plate boundaries. The abbreviations are as follows: FSC (Futuna Spreading Center), NWLSC (Northwest Lau Spreading Center), RR (Rochambeau Rifts), PR (Peggy Ridge), LETZ (Lau Extensional Transform Zone), CLSC (Central Lau Spreading Center), MTJ (Mangatolu Triple Junction), FRSC (Fonualei Rift and Spreading Center), and NELSC (Northeast Lau Spreading Center). The two dashed boxes denote the study areas for this paper covered by Figures 2, 5, and 11, respectively.

elevated $^3He/^4He$ ratios appear to be confined to the NWLSC-RR system.

[5] *Natland* [1980] was the first to propose that clockwise rotation of the Tonga Arc requires tearing of the downgoing Pacific Plate along the northern part of the subduction zone. *Turner and Hawkesworth* [1998] suggested the elevated $^3He/^4He$ ratios found in the RR are due to the ingress of some component of the Samoan mantle plume into the northern Lau Basin through this tear in the plate. Although Samoan lavas exhibit a wide range of geochemical signatures, Samoa does appear to be a "high-^3He" hot spot as evidenced by $^3He/^4He$ ratios ranging from 12 to 24 R_a for lavas from Tutuila, American Samoa [*Farley et al.*, 1992], and up to 33.8 R_a in Samoan lavas from Ofu Island [*Jackson et al.*, 2007]. While the Samoan plume could be the source of the elevated $^3He/^4He$ along the NWLSC-RR, it is also possible that other plume sources to the west could be involved. In either case, the elevated hot spot or ocean island basalt (OIB)-type $^3He/^4He$ signature present along the NWLSC-RR system makes this zone unique among the spreading centers of the northern Lau Basin.

[6] The Tonga – Samoa region is host to a significant water column ^3He plume of unknown origin which is a major hydrographic feature of the south Pacific. Helium profiles collected on a long east–west transect across the Pacific reveal a curious ^3He maximum located in the bathymetric gap between the Samoan Islands and the Tonga-Kermadec Arc [*Lupton et al.*, 2004]. The strongest signal reached δ^3He = 43% at ~1750 m depth at 15°S, 173.1°W over the Tonga Trench (δ^3He is the percentage deviation of the $^3He/^4He$ ratio from the atmospheric ratio). By examining additional profiles, *Lupton et al.* [2004] found that this is a regional plume which extends for over 1000 km to the northwest but is absent at 170°W, only 300 km to the east. The magnitude and depth of the plume indicates that it is not the distal plume from the East Pacific Rise which is weaker (δ^3He = 28%) and lies at 2500 m depth in this area of the south Pacific. Additional helium profiles collected during the past decade have shown that the plume is long-lived and is present all along the northern margin of the Lau Basin over the Tonga Trench between 173°W and 175.5°W, with little variation in strength [*Lupton et al.*, 2011]. The plume overlies a location so deep (>4000 m) and so distant from active volcanoes that it must be the "far-field" plume from a strong and persistent source. While the plume may be derived from activity on the flanks of the Samoan Islands, another likely source is hydrothermal activity in the northern Lau Basin.

[7] The northeastern Lau Basin has been the subject of several studies involving water column measurements and submersible dives [*German et al.*,

2006; *Kim et al.*, 2009]. Recently, an active eruption was observed in progress on West Mata volcano [*Resing et al.*, 2011], and evidence for eruptive activity was also found along the NELSC [*Baker et al.*, 2011]. In contrast, very little is known about the hydrothermal systems of the NWLSC and RR farther west. In this paper, we present the results of the first water column hydrothermal plume survey of the Northwest Lau Backarc Basin conducted in 2008 aboard the *R/V Southern Surveyor.* We also discuss data collected in 2010 aboard the *Dorado Discovery* that provide additional information about hydrothermal venting on the Rochambeau Rifts.

2. Sampling and Analytical Methods

[8] The samples analyzed in this study were collected during the NoLauVE voyage SS07/2008 (http://www.marine.csiro.au/nationalfacility/voyagedocs/2008/MNF-SS07-08_sum.pdf) of the Australian Marine National Facility (R. Arculus, Chief Scientist; *R/V Southern Surveyor*) during April–June 2008. The samples were collected using a rosette fitted with 10 L sampling bottles, a Seabird SBE911 CTD (conductivity-temperature-depth) system, and a SeaTech CST-775DR transmissometer with a 25 cm path length. A total of 54 vertical hydrographic casts were completed during the expedition. This paper will focus on the 20 vertical casts completed along the NWLSC-RR system. In addition to in situ measurements of conductivity, temperature, pressure, and suspended particles, discrete samples were collected for shipboard pH measurements, and for shorebased analysis of helium isotopes and trace metals.

[9] Our primary real-time indicator of hydrothermal activity was the transmissometer mounted on the CTD-rosette which detected suspended particles by measuring the percentage of light transmission (%T) over the 25 cm path length of the transmissometer. The %T for backgroundwater in this region was variable, falling between ~93 and 94%, and therefore we had to adjust our %T "baseline" from cast to cast. However, within a single cast, changes in %T (Δ%T) as small as 0.05%T were significant for indicating the presence of hydrothermal particle plumes. The transmissometer signal decreases when there is an increase in the number of suspended particles. For this reason, we have chosen to plot the *negative* of %T in the figures so that an increase in suspended particles will produce a positive excursion along the *x* axis in concert with the other hydrothermal properties.

[10] The other primary indicator of hydrothermal plumes is the isotopic ratio of helium dissolved in the seawater. The $^3He/^4He$ ratio in the Earth's mantle is enriched by an order of magnitude above that in the atmosphere, making ^3He a uniquely unambiguous indicator of magmatic activity. Because both isotopes of helium are stable and conservative, helium is only removed from the oceanic water column by ventilation into the atmosphere. Thus it is typical for a regional "background" inventory of helium to develop in a basin affected by hydrothermal input of mantle helium. Another source of ^3He in the oceans is the decay of radioactive tritium (^3H), which decays to ^3He with a mean life of 18 years. However, tritium was not a significant source of ^3He for the samples discussed here, since tritium levels are vanishingly small below 1000 m depth in the southern hemisphere. Water samples for helium isotopes were sealed into copper tubing using a special hydraulic crimping device [*Young and Lupton*, 1983]. Over 100 samples for helium analysis were collected as part of this survey. Helium isotope ratios were measured at NOAA's Pacific Marine Environmental Laboratory (PMEL) in Newport, Oregon using a dual-collector mass spectrometer designed specifically for helium measurements [*Lupton*, 1990]. The precision for $^3He/^4He$ measurements was about 0.2% (1-sigma) in δ^3He.

[11] Samples for trace metal analysis were collected in Nalgene bottles during the expedition and archived at CSIRO (Commonwealth Scientific and Industrial Research Organisation, Victoria, Australia). Both filtered (0.4 micron filter) and whole water samples were collected. These samples were archived for ~two years prior to being shipped to PMEL in Seattle, where they were acidified with sub-boiling distilled 6N HCl to pH ≈ 1.7. They were subsequently stored for one month prior to analysis for Fe and Mn. Iron was determined as a direct injection modification of *Measures et al.* [1995], while Mn was determined by modifying the direct injection technique of *Resing and Mottl* [1992] by adding 4 g of nitrilo-triacetic acid to each liter of buffer. Fe and Mn are both highly enriched in typical hydrothermal fluids, and therefore are useful water column tracers for detecting hydrothermal plumes [e.g., *Resing et al.*, 1999].

[12] Bathymetric mapping of the Northwest Lau Backarc Basin was undertaken with a Simrad EM300 multibeam system, mounted on the hull of the *R/V Southern Surveyor*, comprising a 1° by 1° set of 135 beams clustered around a 30 kHz frequency. Real-time beam steering compensation was

made for ship motion. Motion sensing and positional navigation had accuracies of ≤0.02° and ±5 m, respectively. Bathymetry and backscatter data were edited and gridded on-board at a variety of cell sizes with *Caris* software.

[13] For the repeat visit to the RR conducted in 2010 aboard the *Dorado Discovery*, the sampling package consisted of a standard CTD rosette system fitted with an altimeter, 2 nephelometers, and 2 ORP (oxidation-reduction-potential) sensors. A nephelometer responds to suspended particles by measuring light backscattering, and has greater sensitivity than the transmissometer used during the 2008 survey. The nephelometer response in volts is equivalent to nephelometer turbidity units (NTU), and ΔNTU is the value above ambient nonplume water. In addition to these in situ measurements, discrete samples were collected for shipboard analysis of pH, and for helium isotopes. The helium samples were collected in the same manner as in the 2008 expedition using the hydraulic crimping device and analyzed at the NOAA/PMEL Helium Isotope Laboratory in Newport, Oregon.

[14] A complete listing of all the station locations and analytical results is given in Table S1 and S2 in the auxiliary material.[1]

3. Results

3.1. Northwest Lau Spreading Center

[15] The NWLSC has a fairly simple geometry with the spreading axis clearly defined by a sinuous axial high that extends from 15°30′ S down to 16°10′ S (Figure 2). At latitude ∼15°54′ S a caldera collapse feature (Southern Caldera) is present on the axial high of the spreading axis (Figure 3). A similar feature called Central Caldera is present at latitude ∼15°48′ S where the spreading axis shoals to a depth of 2000 m, and at its shallowest point is marked by a clear caldera collapse feature about 100 m deep (Figure 4). A total of 10 hydrocasts were completed along the NWLSC, with four of these positioned in or near the Central Caldera, one in Southern Caldera, and the remainder distributed along the spreading axis (Figures 2 and 4). The two casts on the southern end of the spreading center (NLH-33 and -34) close to the Peggy Ridge do not show evidence of local hydrothermal input: the %T and TMn profiles are nearly constant versus depth, and the ^{3}He profiles increase smoothly to values of δ^3He = 40% at 2000 m depth. In fact, while these two profiles serve to define the regional δ^3He background, it is worth noting that δ^3He = 40% represents a considerable ^{3}He excess above typical background values for the southwestern Pacific, which average about δ^3He = 25% at 2000–2500 m depth [*Lupton et al.*, 2004]. Thus the deep water column along the entire NWLSC–RR system has a high ^{3}He background due to the cumulative effect of the hydrothermal venting in the region.

[16] The NWLSC is very hydrothermally active with seven of the ten hydrocasts revealing evidence for hydrothermal input. Hydrothermal activity in the Southern Caldera was revealed by a sharp decrease in light transmission, TMn, and δ^3He at depths below 2000 m in cast NLH-30, which was positioned near the western caldera wall (Figure 3). The caldera has a floor at ∼2160 m depth with a steep western wall reaching up to ∼2000 m and an eastern wall that is virtually absent with a sill at ∼2130 m depth. It is notable that the 2000 m depth of the plume top coincides with the depth of the caldera's western rim. Taken together, this indicates that hydrothermal venting is taking place within the caldera producing a ^{3}He- and particle-rich plume. This plume appears to be advected to the northwest by ocean currents where it is, at least partially, trapped by the steep western wall of the caldera. The shape of the ^{3}He, %T, and TMn profiles here is consistent with the presence of low temperature diffuse venting, which does not typically produce high-rising plumes disconnected from the seafloor.

[17] Four hydrocasts within Central Caldera exhibited strong signals in both %T and excess ^{3}He, with δ^3He reaching a maximum of 70 to 100% at 1900–2000 m depth in all four profiles (Figure 4). For casts NLH-29, -31, and -32, TMn varies in concert with δ^3He and %T. The bathymetric depth of the seafloor surrounding the caldera averages 2000 m on the northwestern rim and 2040 m on the southwestern rim (Figure 4). The caldera floor is 80 m deeper, averaging 2100 m depth and reaching 2200 m in a few spots. Unlike the Southern Caldera, which is breached to the east, the Central Caldera is completely closed at depths below 2040 m. Hydrocast NLH-29 was positioned on the western rim of the caldera and had the weakest hydrothermal signals of the four casts. This suggests that the plume source is likely somewhere within the caldera, but also shows that the plume is not trapped within the caldera but has ascended above the caldera walls. The other three hydrocasts, and NLH-28 and NLH-32 in particular, exhibit the

[1] Auxiliary materials are available in the HTML. doi:10.1029/2011GC003891.

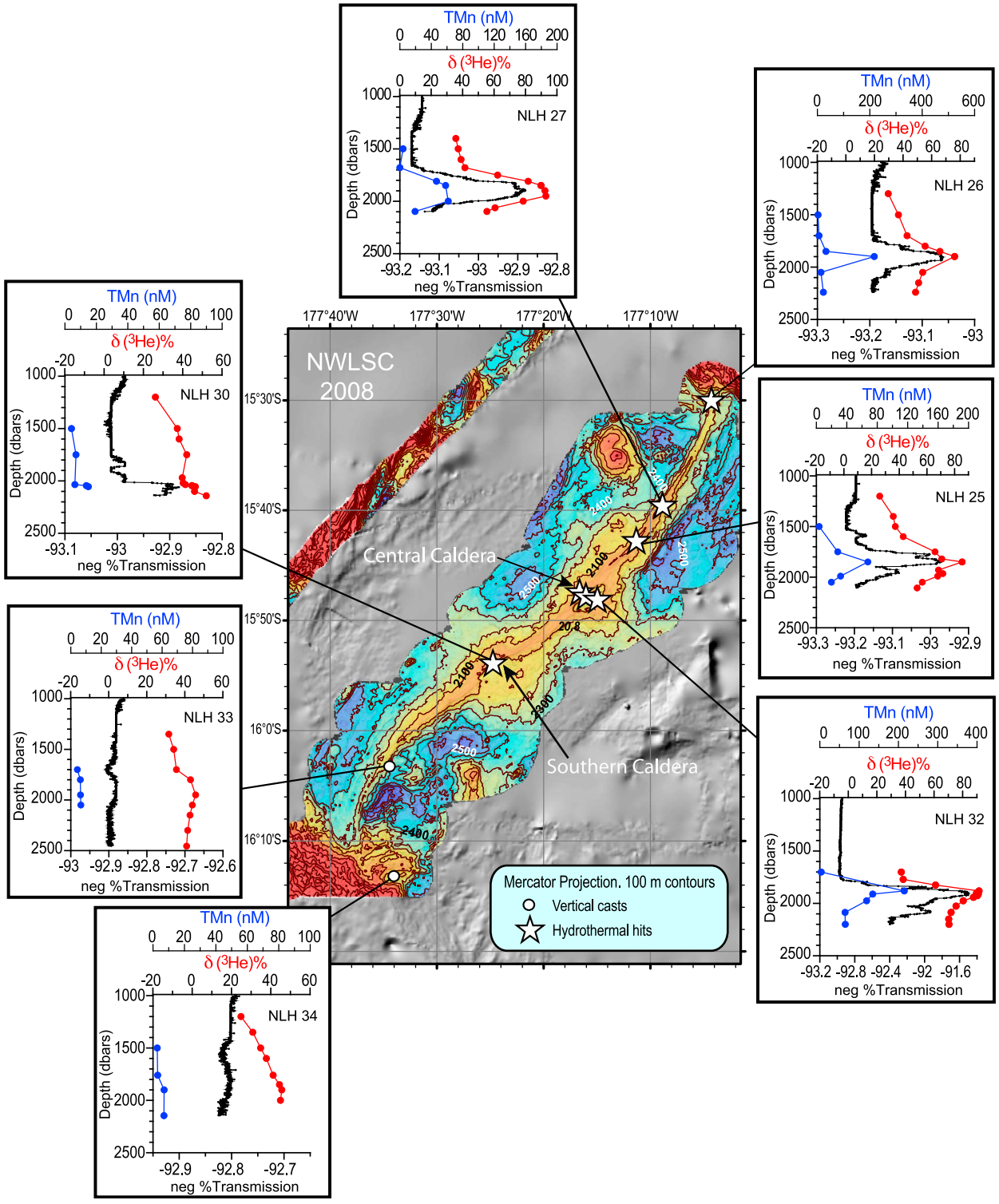

Figure 2. Map summarizing the 2008 hydrocast results for the Northwest Lau Spreading Center (NWLSC). The stars denote locations of hydrocasts that clearly detected hydrothermal activity. The insets show vertical profiles of δ^3He, total Mn, and %T (suspended particles) plotted versus depth. Note variable scales are used in these insets. We have reversed the *x* axis for the %T because a decrease in %T corresponds to a higher concentration of suspended particles.

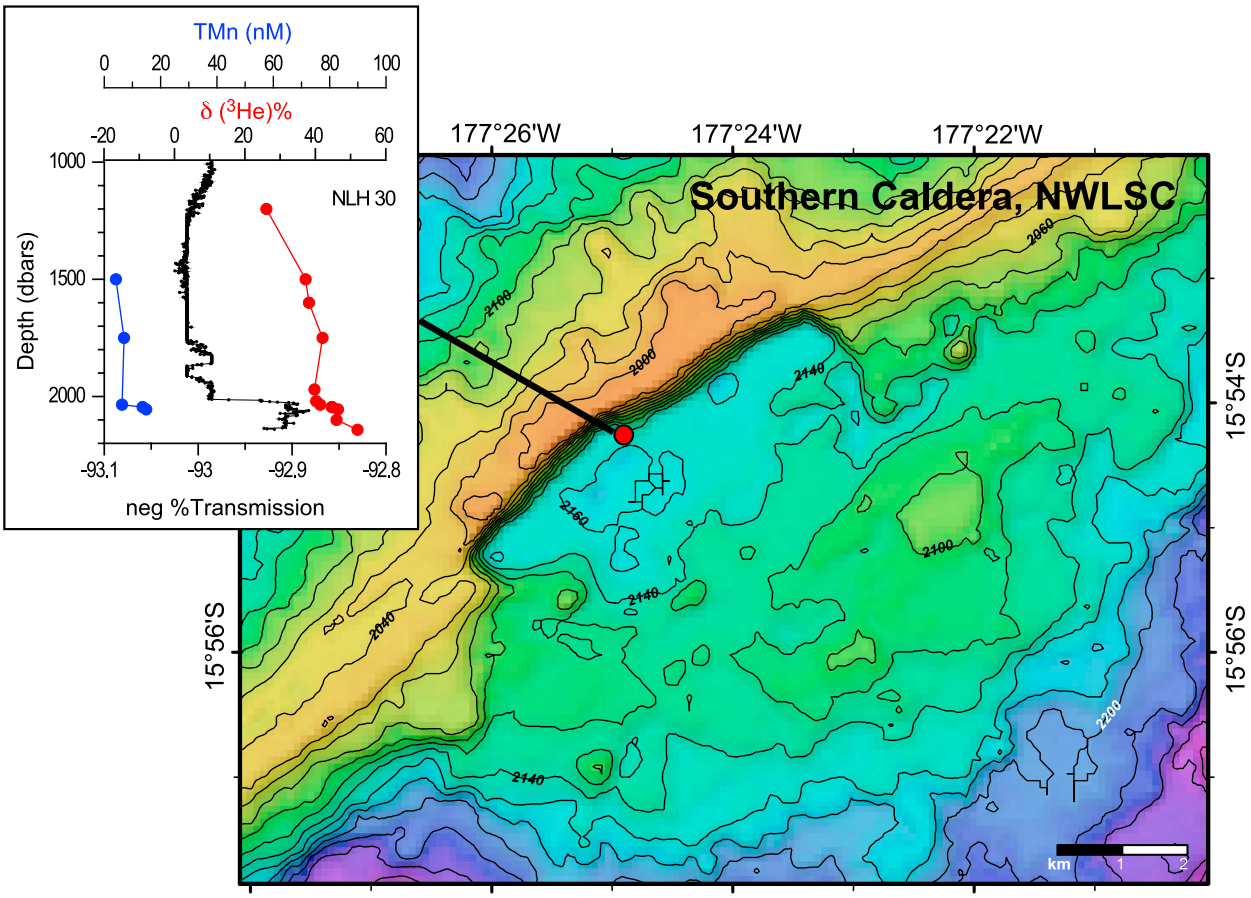

Figure 3. Detail map of the Southern Caldera on the NWLSC showing the location for cast NLH-30. The inset shows vertical profiles of δ^3He, total Mn, and %T (suspended particles) plotted versus depth.

classic plume profile associated with high-temperature black smoker-type venting, i.e., the plume signals reach a maximum some distance up in the water column rather than at the seafloor. This type of profile is indicative of a plume produced by a strong buoyancy flux that has deposited hydrothermal effluent (particles and ^{3}He) into a neutrally buoyant layer some hundreds of meters above the seafloor. Based on the strength and shape of these four profiles, we conclude that there is likely high temperature venting somewhere within the Central Caldera.

[18] The three profiles along the northern section of the NWLSC (NLH-25, -26, and -27) show robust hydrothermal plumes with δ^3He reaching a maximum of 76 to 90% at ~1900 m depth and Δ%T and TMn signals that vary in concert with the ^{3}He (Figure 2) . Compared to the profiles within Central Caldera (Figure 4), these three profiles to the northeast of Central Caldera have the same depth of plume maximum, and indistinguishable ratios of Fe to ^{3}He and Mn to ^{3}He. The intensity of the plume at NLH-27 (δ^3He = 90%) located 20 km away from Central Caldera is equal to the values of δ^3He = 67–95% detected within Central Caldera (Figure 4). Given that one would expect some dilution of the plume signal with distance from the source, this suggests the existence of a separate hydrothermal source northeast of Central Caldera. However, the matching plume depth and chemical characteristics argue that NLH-27 and the other northern stations have simply detected the far-field plume advected away from Central Caldera with relatively little dilution.

3.2. Rochambeau Rifts

[19] In contrast to the relatively simple bathymetric structure of the NWLSC, the RR consists of a complicated suite of ridges and pull-apart basins. Our survey consisted of 12 vertical hydrocasts scattered throughout the region (Figure 5). One of the prominent features of the RR is the volcanic edifice known as Lobster Caldera at latitude 15°20′ S, which rises to a depth of 1400 m, several

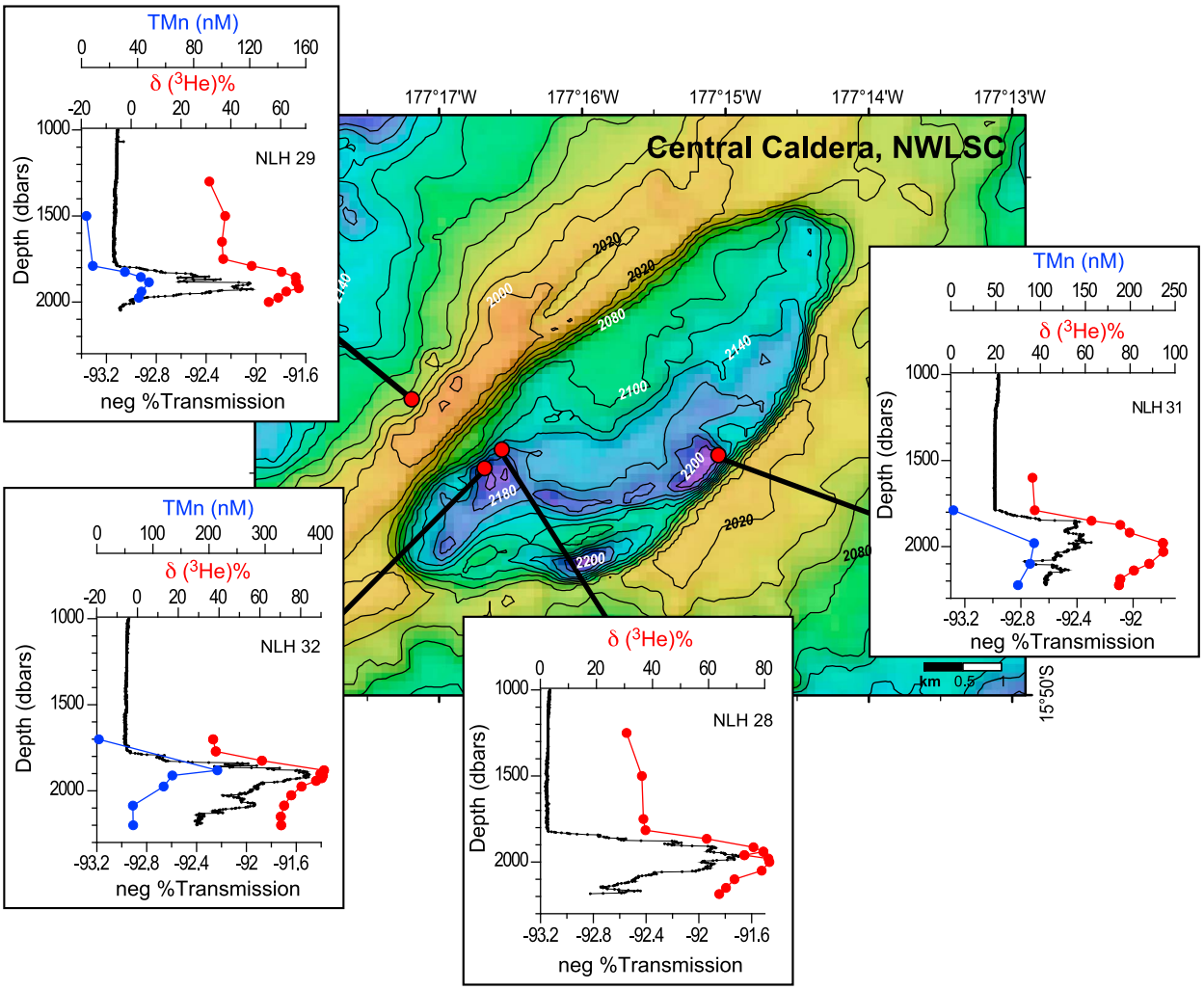

Figure 4. Detail map of the Central Caldera on the NWLSC showing locations and profiles for casts NLH-28, −29, −31, and −32. The insets show vertical profiles of δ^3He, total Mn, and %T (suspended particles) plotted versus depth.

hundred meters above the surrounding topography. The summit of Lobster is marked by a circular caldera with walls about 100 m high on the west side and an average depth of about 1500 m in the caldera floor (Figure 6). By contrast, the eastern wall of the caldera is virtually absent, rising only ∼20 m above the caldera floor with the eastern rim averaging 1480 m depth. The two hydrocasts we completed within the caldera (NLH-18 and -19) detected the highest δ^3He and Δ%T of the entire expedition, with δ^3He reaching maximum a value of 239% in the bottom bottle of cast NLH-19 located near the western wall. Both profiles show a more or less continuous plume presence from 1400 m depth down to the seafloor at 1500 m. Curiously, for both hydrocasts the maximum Δ%T occurs about 80 m above the seafloor at ∼1420 m depth, while the highest δ^3He is found very near the bottom. The TMn profiles vary to a large extent in concert with δ^3He. This implies two different styles of venting producing different plume layers, i.e., ^{3}He-rich diffuse venting producing the low-lying plume, and particle-rich high-temperature venting producing the upper plume. Except for the upper most sample in NLH-19 at 1387 m with a δ^3He of 93%, it is notable that the plume signals detected in casts NLH-18 and NLH-19 are mostly absent at depths shallower than ∼1400 m, with the result that the center of the plume does not extend above the western rim of the caldera. However, the eastern caldera walls rise only 20 m above the caldera floor, thus any portions of the plume shallower than ∼1480 m could escape to the east.

[20] The profiles from the remaining casts are more difficult to interpret. Three of the casts (NLH-14, -16, and -24) have essentially no hydrothermal plume signal with δ^3He consistent with the

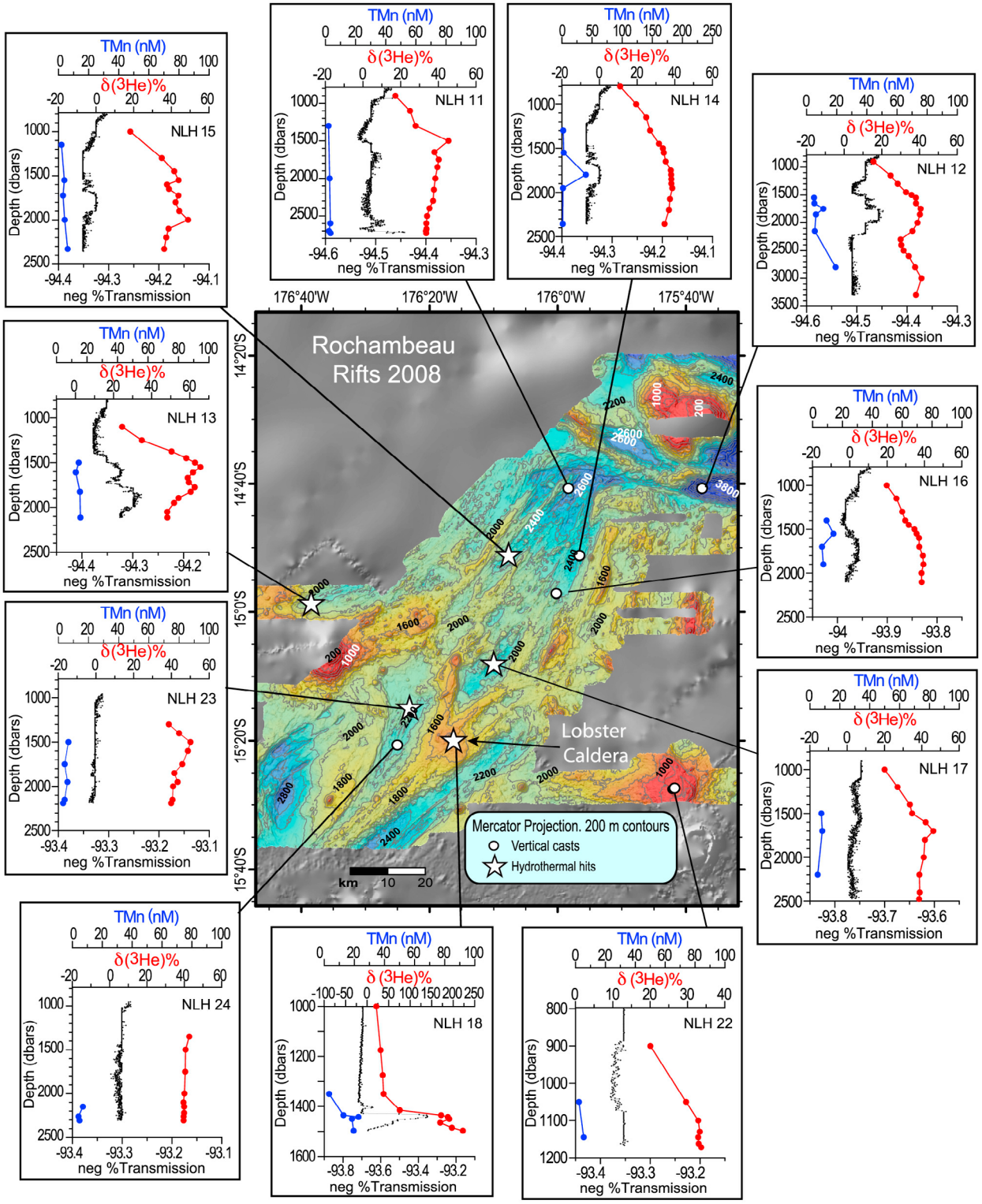

Figure 5. Map summarizing the 2008 hydrocast results for the Rochambeau Rifts (RR). The insets show vertical profiles of δ^3He, total Mn, and %T (suspended particles) plotted versus depth. We have reversed the x axis for the %T because a decrease in %T corresponds to a higher concentration of suspended particles.

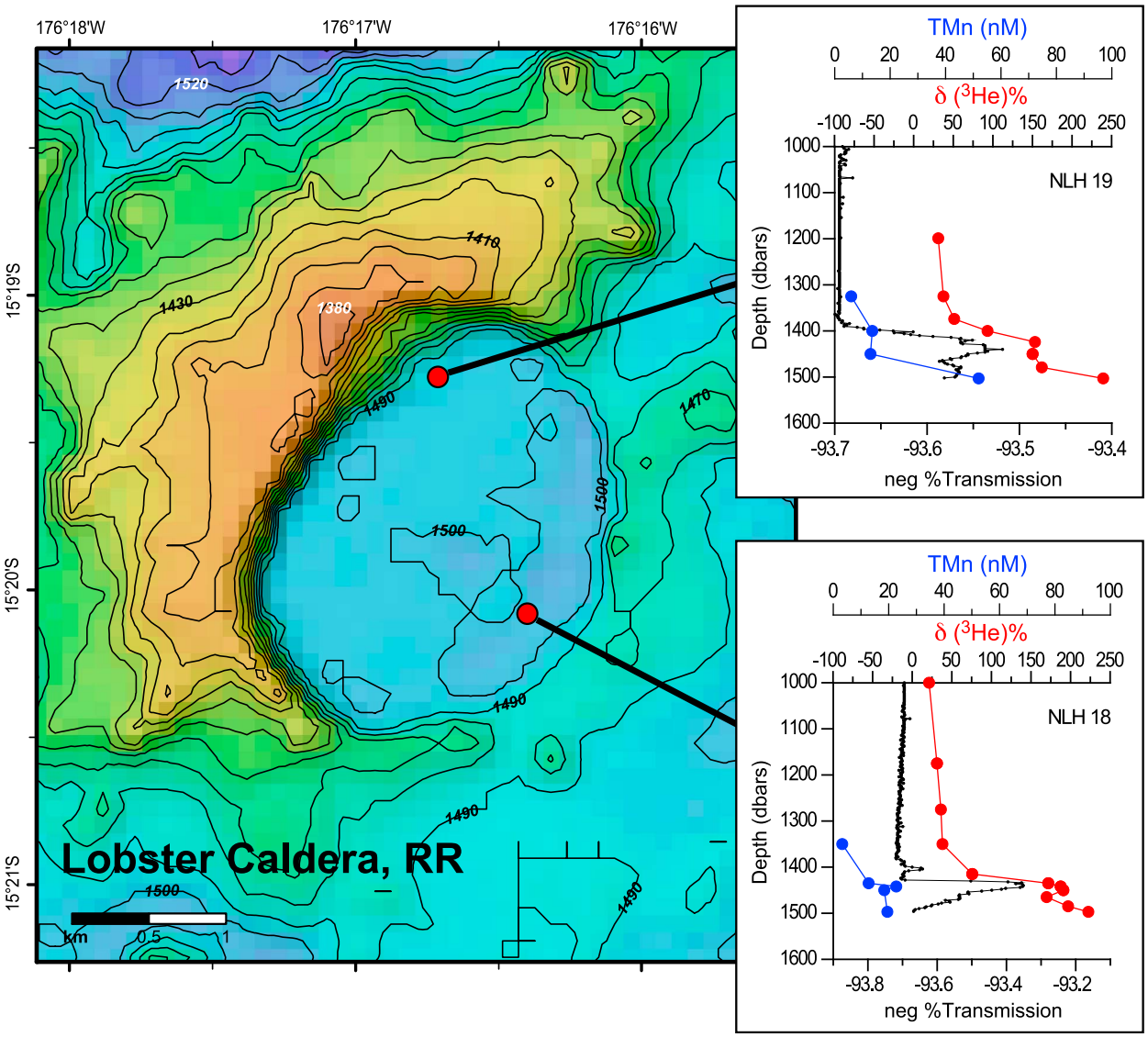

Figure 6. Detail map of Lobster Caldera on the Rochambeau Rifts showing locations and profiles for casts NLH-18 and −19. The insets show vertical profiles of δ^3He, total Mn, and %T (suspended particles) plotted versus depth.

regional background, but in several other casts (NLH-11, -13, -15, -17, and -23) there is a small but clear maximum in δ^3He at ~1500–1700 m depth. However, these casts lack any clear excess in TMn or Δ%T. In addition to Lobster Caldera, there are several other bathymetric highs in the region that could host hydrothermal systems capable of producing plumes at that depth. Another interpretation is that this 1500 m deep signal is simply the far-field plume emanating from Lobster Caldera. The one exception might be NLH-13, northwest of Lobster Caldera and on the northern flank of Rochambeau Volcano, which detected two strong ^{3}He maxima, one reaching δ^3He = 65% at 1550 m depth and a second slightly weaker maximum (δ^3He = 62%) at 1775 m depth. Considering the strength of these ^{3}He signals, the considerable (57 km) distance from Lobster Caldera, and the existence of shallow topography up to 1000 m depth intervening between Lobster and the cast location, the double plume at NLH-13 is likely from a source other than Lobster Caldera, and potentially from Rochambeau itself. Certainly the deeper (1775 m) δ^3He maximum cannot be attributed to venting on Lobster Caldera. Surprisingly, station NLH-24 just 16 km west of Lobster shows no sign of a δ^3He maximum at 1500 m depth, suggesting that the regional currents may be carrying the Lobster Caldera plume northward. In addition to having a maximum in δ^3He at 1500 m depth, station NLH-15 in the northern basin

has another distinct maximum reaching δ^3He = 49% at 2000 m depth, suggesting a deep hydrothermal source in that basin. However, none of the other stations in that basin (NLH-11, -14, and -16) show a ^{3}He plume at that depth.

[21] Two other hydrocasts that were located on the periphery of this region deserve separate treatment. NLH-22 was a shallow cast into Dugong Volcano ~50 km southeast of the RR located on a NNW–SSE-trending ridge which includes the subaerial volcano of Niuafo'ou (Figures 1 and 5). Although the transmissometer did not detect a significant suspended particle signal, δ^3He for NLH-22 increases smoothly with depth reaching a value of 33.7% near the bottom at 1172 m depth. Comparison with a typical background profile (NLH-14) shows that the δ^3He for cast NLH-22 is about 8% higher than the regional background, suggesting that Dugong Volcano may host moderate hydrothermal activity. We also completed a deep cast (NLH-12) in a channel northeast of the RR (Figure 5). This channel has an unobstructed connection to the West-East-trending Tonga Trench, and despite its distance from the RR, the cast had two maxima in ^{3}He, one reaching δ^3He = 41% at 1750 m and another deeper maximum of δ^3He = 41% at 3000 m depth. The shallower δ^3He maximum at 1750 m depth is accompanied by a maximum in suspended particles (Δ%T). The δ^3He maximum at 1750 m does not appear in any of the other casts completed during this expedition, suggesting it is not related to the spreading activity along the NWLSC–RR system. However, a similar δ^3He maximum has appeared in several casts completed previously north of the Lau Basin on the slopes of the trench. Thus this signal may be another expression of the pervasive plume at 1750 m depth discussed previously by *Lupton et al.* [2004].

3.3. Trace Metals

[22] For any individual hydrocast, TMn and TFe concentrations vary in concert, and either of these trace metals serve equally well for the purposes of hydrothermal plume detection. For this reason, we have chosen to plot only TMn versus depth in Figures 2 through 6. However, the specific relationships between TFe, TMn, and ^{3}He vary with locality. One parameter of particular interest is the end-member Fe/Mn ratio. Acidic, CO_2-rich hydrothermal fluids such as those found on hot spot volcanoes have elevated Fe/Mn ratios, while typical MOR hydrothermal fluids have lower Fe/Mn ranging from 0.5 to 5.0 [*Von Damm*, 1995]. For example, Loihi Seamount has high Fe concentrations with Fe/Mn ratios varying from 22 to 46 [*Sedwick et al.*, 1992]. Because of the OIB or hot spot influence present in the Northwest Lau Backarc Basin, one might expect the hydrothermal fluids to have elevated Fe/Mn similar to Loihi Seamount. Figure 7a shows that, while there are considerable differences in the Fe/Mn ratios at Lobster Caldera compared to samples from Central Caldera on the NWLSC, all of the Fe/Mn values fall within the normal range for MOR-type spreading centers [*Von Damm*, 1995]. Specifically, Fe/Mn averages about 4.0 at Lobster Caldera, a factor of 5 higher than at Central Caldera, where Fe/Mn = 0.82 (Figure 7a).

[23] Lobster Caldera and Central Caldera also have much different volatile-to-metal ratios in the fluids as indicated by the ^{3}He/Mn ratios at these two sites. As shown in Figure 7b, Lobster Caldera has an estimated end-member ^{3}He/Mn of 1.3×10^{-7}, while Central Caldera has ^{3}He/Mn of 8.8×10^{-9}, a factor of 15 lower. These ^{3}He/Mn values fall within the range of typical MOR hydrothermal plumes, which vary from 6×10^{-9} up to 2×10^{-7} [e.g., *Urabe et al.*, 1995]. It is notable that Lobster Caldera has ^{3}He/Mn similar to that at the 9°45′ N East Pacific Rise site (^{3}He/Mn = 1.2×10^{-7}), which is known to have been perturbed by magma input [*Lupton et al.*, 1993], while the ^{3}He/Mn at Central Caldera is similar to that at longer-lived mature sites [e.g., *Lupton et al.*, 1993; *Massoth et al.*, 1994]. As discussed below, the Lobster Caldera plume has elevated ^{3}He/heat, suggesting recent magmatic activity. The plumes at Central Caldera had high rise height consistent with focused high-temperature black smoker-type venting that would mobilize and transport metals, resulting in lower ^{3}He/Mn. Lobster Caldera had plumes with relatively low rise height, probably produced by low-temperature diffuse venting likely to have higher gas content and higher ^{3}He/Mn.

3.4. Repeat Survey of Rochambeau Rifts in 2010

[24] In November of 2010, Bluewater Metals (South Pacific) Ltd. conducted a water column survey of the RR aboard the *Dorado Discovery*, providing another assessment of hydrothermal activity in this region approximately two years after the earlier work of the *R/V Southern Surveyor*. The *Dorado Discovery* completed two vertical casts and three tows on the southern part of the RR, concentrating on Lobster Caldera and the surrounding area. In the

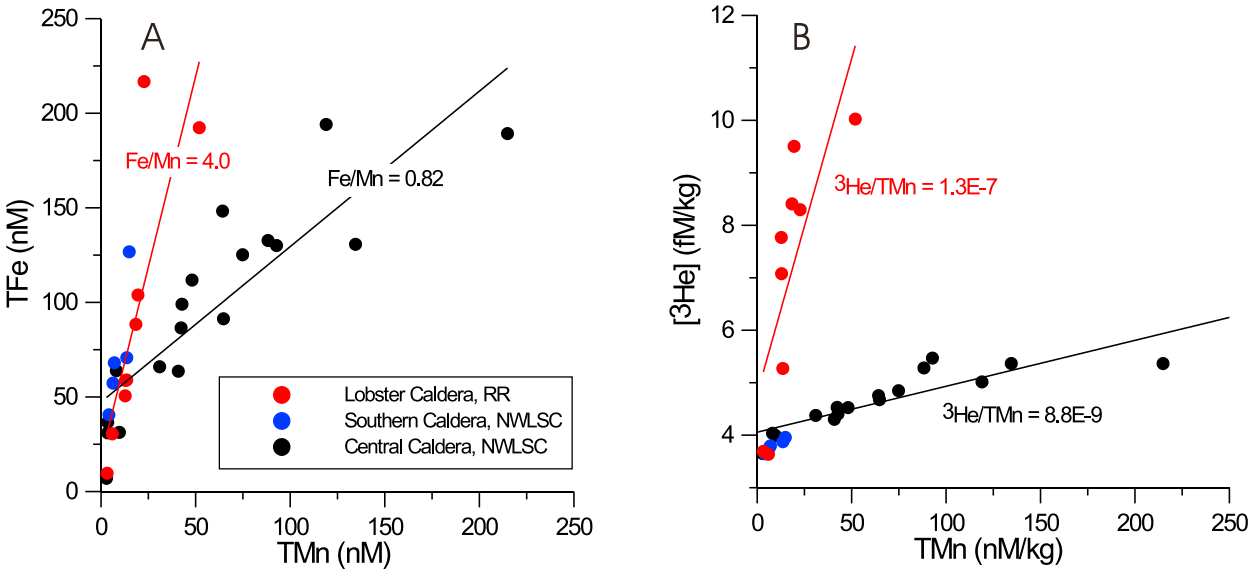

Figure 7. (a) Total Fe versus Total Mn for samples from Lobster Caldera, RR (red), Southern Caldera, NWLSC (blue) and Central Caldera, NWLSC (black). Linear regression fits for Lobster Caldera and Central Caldera gave slopes of Fe/Mn = 4.0 and 0.82, respectively. (b) ^{3}He concentration versus Total Mn. Symbols same as in Figure 7a. Linear regression fits for Lobster Caldera and Central Caldera gave slopes of ^{3}He/TMn = 1.3 × 10^{-7} and 8.8 × 10^{-9}, respectively.

discussion which follows, we concentrate on helium and nephelometer data, since these are the most sensitive indicators of hydrothermal activity.

[25] An extensive tow (DD-54T) over Lobster Caldera crossed the caldera three times (Figure 8). We have divided the tow into three segments designated A, B, and C corresponding to the three crossings of the caldera. Strong suspended particle anomalies within the caldera were observed on all three segments (Figure 9), indicating the presence of hydrothermal activity within Lobster Caldera. While most of these suspended particle signals were confined to the caldera proper, the western end of tow 54T-Part B detected a suspended particle plume at 1350–1400 m depth outside the caldera perimeter. Tow 54T-Part A also detected a plume outside and just above the rim depth of the caldera. It is not clear whether this is a caldera plume escaping to the west, or a plume generated by a separate hydrothermal source on the western flanks of the volcano.

[26] A total of 11 discrete samples were collected on tow 54T, and several of the samples were highly enriched in δ^3He (Figure 10a). In particular, the sample from bottle 8 on tow 54T-Part C had δ^3He = 359%, higher than the maximum δ^3He of 239% detected in this locality during the 2008 *Southern Surveyor* expedition (Figures 9c and 10a). This difference probably reflects the randomness of the sampling process rather than indicating an increase in hydrothermal activity between 2008 and 2010. Nonetheless, the fact that highly enriched samples were collected in 2010 allows us to make more accurate estimates of the characteristics of the end-member ^{3}He/^{4}He ratio, which is discussed in section 3.5. Another property ratio of interest is the relationship between helium and heat. Figure 10b is a plot of [^{3}He] concentration versus temperature anomaly $\Delta\theta$ for the DD-54T samples collected at Lobster Caldera. The temperature anomaly $\Delta\theta$ is the excursion (in °C) from the background potential temperature profile as defined by a linear fit of potential temperature θ versus potential density σ_θ. Although there is considerable scatter in the plot, the fit gives a slope of [^{3}He]/$\Delta\theta$ of (6.0 ± 0.1) × 10^{-12} ccSTP/cal, or (6.4 ± 0.1) × 10^{-17} mole/J.

[27] It has been shown that $\Delta\theta$ in the neutrally buoyant plume underestimates the actual enthalpy added to the water column because of the entrainment of colder deep water into the rising buoyant plume [*McDougall*, 1990]. The relationship of $\Delta\theta$ to enthalpy is also affected when the salinity of the vent fluids introduced at the seafloor differs from that of ambient seawater [*McDuff*, 1995; *Lavelle et al.*, 1998]. Since we have no information on the salinity of the vents fluids issuing from Lobster Caldera, we assume that it is close to seawater salinity and confine ourselves to the entrainment

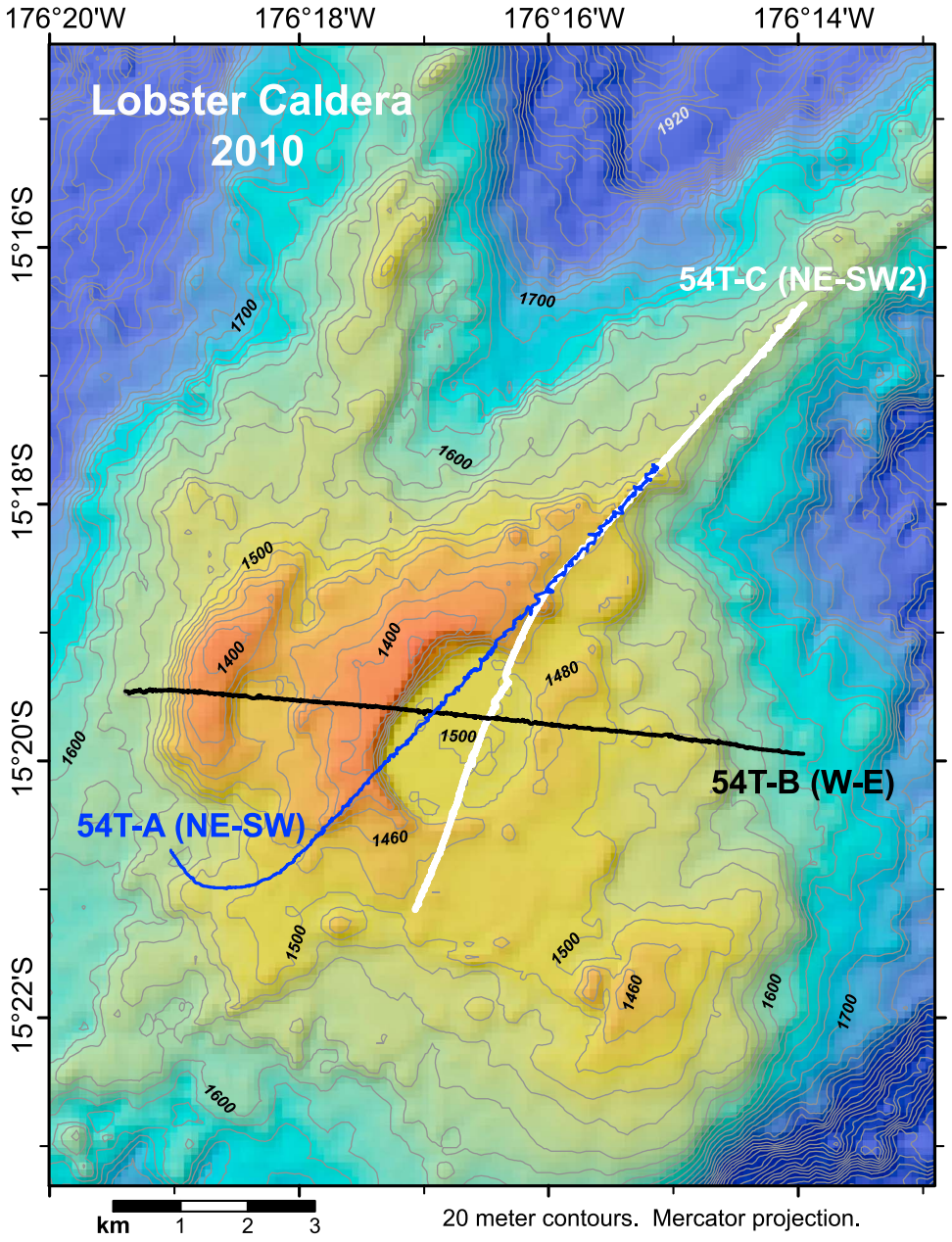

Figure 8. Map of Lobster Caldera on the Rochambeau Rifts showing the track of tow DD-54T completed in 2010 by the *Dorado Discovery*. For clarity we have divided this long tow into parts A, B, and C. Note that only the portions of the tow near the Lobster Caldera summit are shown.

correction. The entrainment correction as derived by *McDougall* [1990] is [1/(1 − R)], where R = [(α/β)*(dθ/dS)] and α and β are, respectively, the thermal coefficient of expansion and the haline coefficient of contraction. For the deep water column of the NWLSC, R = −2.0, giving a correction factor of 1/3. Therefore the actual heat that has been added to the plume layer is 3 times higher than indicated by $\Delta\theta$, with the result that the measured ^{3}He/heat ratio should be revised downward to about 2.1 × 10^{-17} mole/J. This is still an elevated ^{3}He/heat value, close to the theoretical ^{3}He/heat ratio for the upper mantle [*Lupton et al.*, 1989] and about 4 times higher than the values of (0.3–0.5) × 10^{-17} mole/J associated with typical steady state hydrothermal systems on mid-ocean ridges [*Lupton et al.*, 1999]. It has been shown that MOR segments that have been recently perturbed by magmatic input have elevated ^{3}He/heat ratios in the hydrothermal fluids [*Lupton et al.*, 1989, 1999]. If we

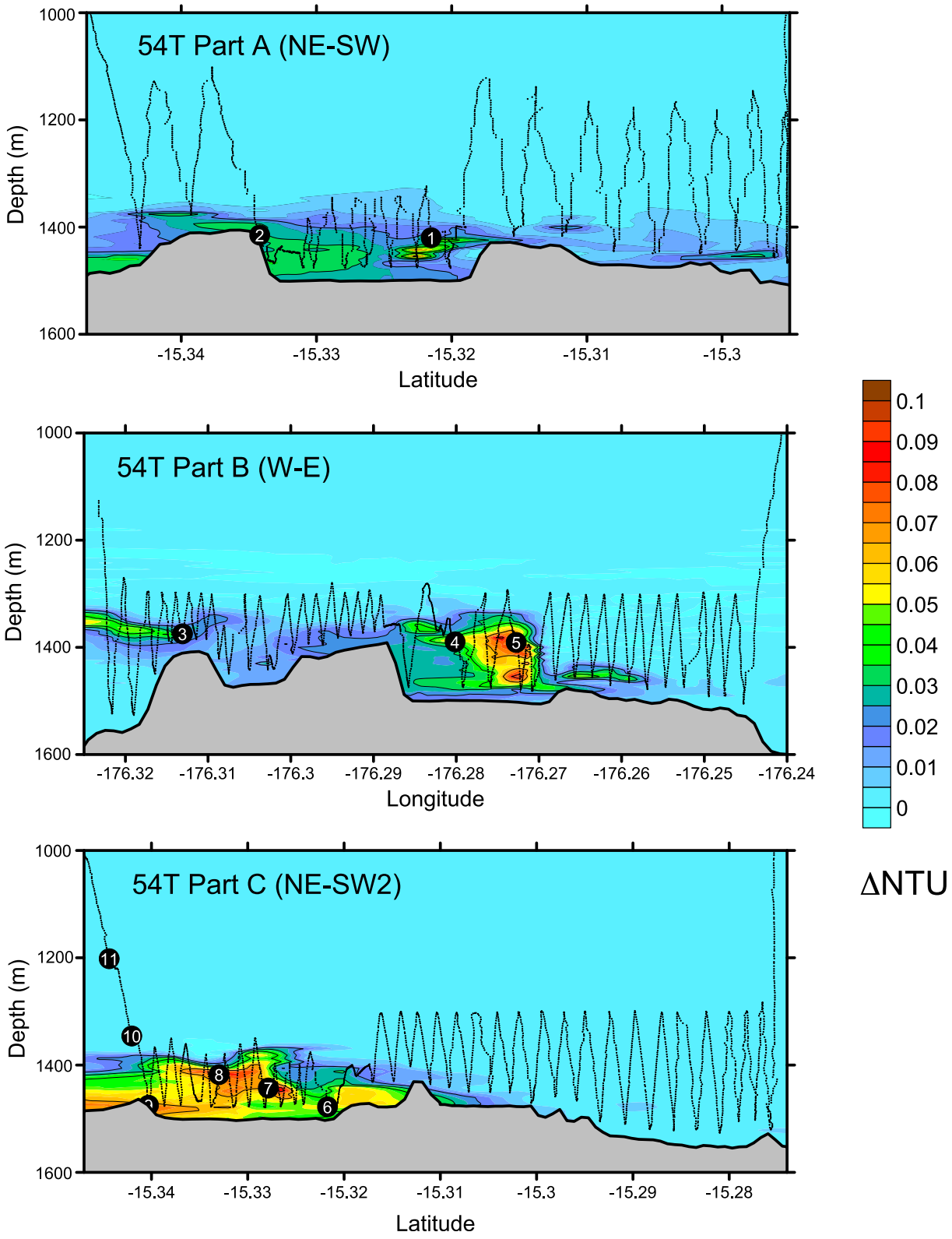

Figure 9. Section view plots of the three parts (A, B, and C) of tow DD-54T completed over Lobster Caldera in 2010. The contours are of the nephelometer (suspended particle) signal ΔNTU. The small dotted lines denote the actual sawtooth pattern of the CTD/rosette package. The black circles denote where the 11 discrete bottle samples were collected, with the numbers denoting the rosette bottle number. The dark black line denotes the seafloor bathymetry under the CTD tow package. Refer to Figure 8 for the track of the tow trajectory over the caldera.

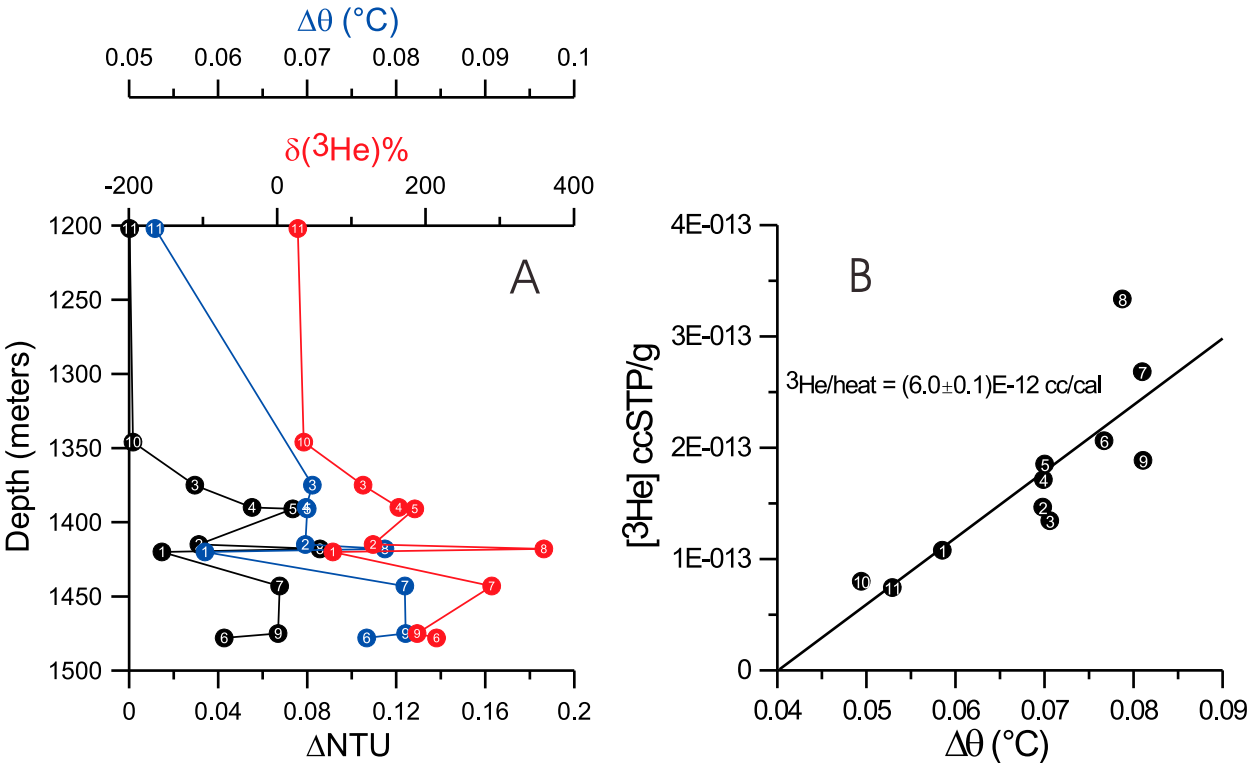

Figure 10. Discrete bottle results for tow DD-54T over Lobster Caldera. (a) Plot of helium isotope ratio δ^3He, nephelometer response ΔNTU, and temperature anomaly $\Delta\theta$ versus depth. Bottle numbers as in Figure 9. (b) Plot of ^{3}He concentration versus temperature anomaly $\Delta\theta$. The linear least squares fit gives an estimate of the ^{3}He/heat ratio of $(6.0 \pm 0.1) \times 10^{-12}$ ccSTP/cal or $(6.4 \pm 0.1) \times 10^{-17}$ mole/J.

assume that backarc spreading centers such as the NWLSC - RR behave in the same way as MOR systems, then the elevated ^{3}He/heat at Lobster Caldera suggests that the hydrothermal system there has been recently influenced by magmatic input.

[28] In addition to the detailed survey of Lobster Caldera provided by tow DD-54T, the *Dorado Discovery* also collected water column data from two vertical casts and two tows surrounding Lobster Caldera (Figure 11). The two tows, DD-56T and DD-58T were relatively short and detected only weak suspended particle signals. Furthermore the discrete bottle samples for 56T and 58T were all collected in a vertical profile as the package was ascending at the end of each tow. As shown in Figure 11, profiles DD-55V, -56T, -57V, and -58T all have excess ^{3}He above the regional background, reaching a maximum of δ^3He = 45–55% at ~1600 m depth. Of these four profiles, DD-56T at about 10 km northwest of Lobster had the strongest δ^3He anomaly, exhibiting a sharp maximum of δ^3He = 54.6% at 1605 m depth. One interpretation is that this maximum in δ^3He is a regional plume produced by the venting in Lobster Caldera. However, the samples collected within the caldera (DD-54T in 2010, and NLH-18 and -19 in 2008) demonstrate that Lobster Caldera is introducing hydrothermal effluent at 1400–1500 m depth, which is shallower than the 1600 m plume depth in the four surrounding casts. The deepest bottles collected within the caldera on DD-54T had a potential density σ_θ of 27.57, whereas the plume maximum detected in cast 56T at 1605 m depth had $\sigma_\theta = 27.59$. The CTD data for cast 56T confirms that σ_θ of 27.57 falls at 1483 m depth, much shallower than the plume maximum. Thus the regional helium plume detected in the four surrounding casts clearly lies on a deeper isopycnal surface than the helium introduced at Lobster Caldera. This suggests that either the Lobster Caldera hydrothermal system is venting very saline fluids dense enough to sink onto a deeper density surface, or that this regional helium plume has come from a different hydrothermal source deeper than Lobster Caldera.

3.5. End-Member Helium Isotope Compositions

[29] When water column samples are sufficiently enriched in helium, it is possible to estimate the

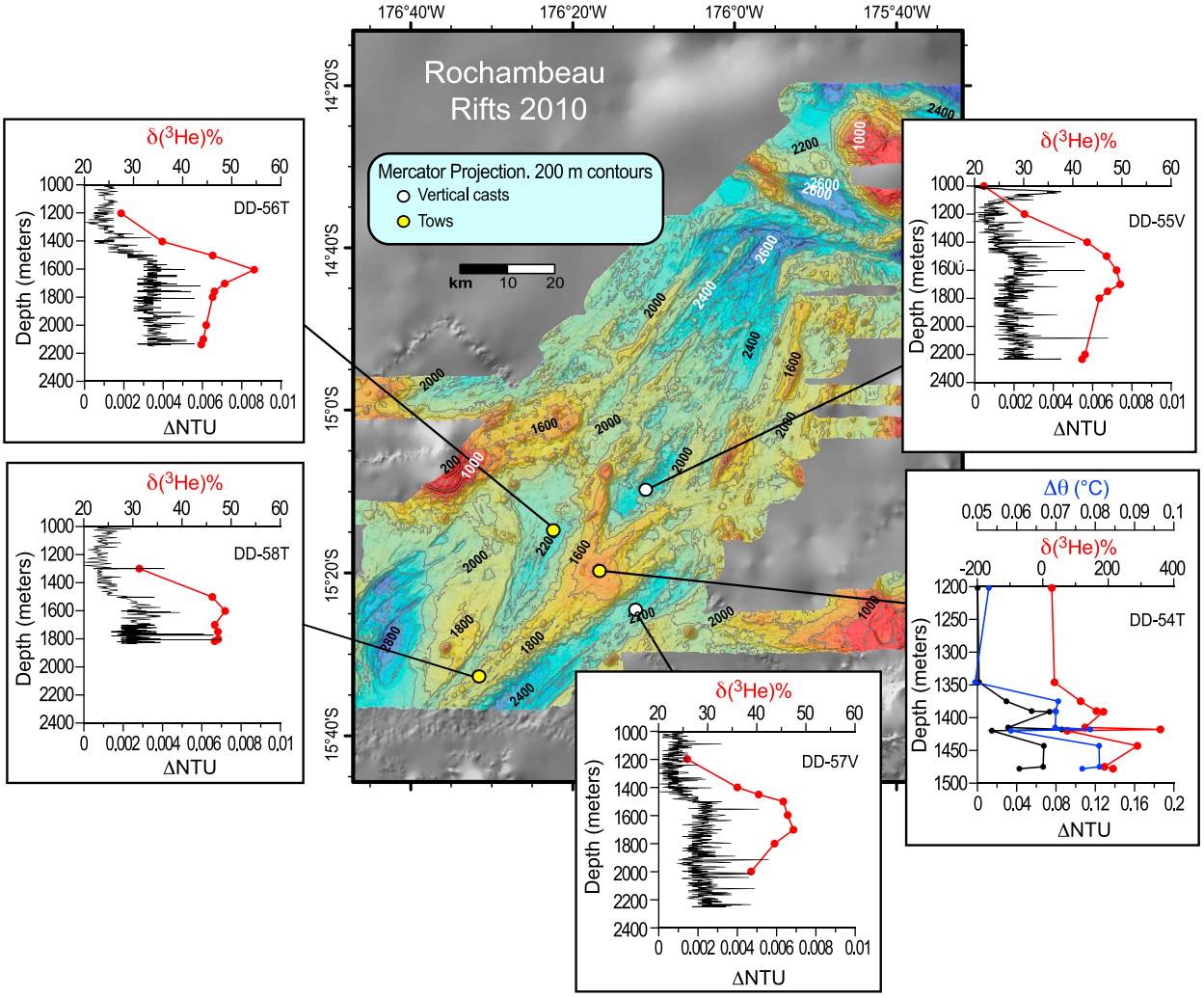

Figure 11. Map summarizing all of the hydrocast results for the Rochambeau Rifts collected by the *Dorado Discovery* in 2010. The insets show vertical profiles of helium isotope ratio δ^3He and nephelometer response ΔNTU plotted versus depth. Tow 54T is summarized by placing all of the discrete bottle data into a vertical profile.

^{3}He/^{4}He ratio of the undiluted source fluid by means of a linear regression fit to [^{3}He] versus [^{4}He]. The slope then gives an estimate of the ^{3}He/^{4}He ratio of the end-member helium which has been added by hydrothermal input. We have done this for two of the areas sampled where the plumes were strong enough to warrant this approach, i.e., the Central Caldera of the NWLSC and Lobster Caldera on the RR. The linear least squares fit to [^{3}He] versus [^{4}He] for casts NLH-18 and -19 in Lobster Caldera yields a slope of $(2.69 \pm 0.061) \times 10^{-5}$ (1-sigma), corresponding to a helium isotope ratio of $R/R_a = 19.3 \pm 0.4$ (Figure 12a). A similar fit to tow DD-54T collected in Lobster Caldera in 2010 gave $R/R_a = 18.7 \pm 1.1$ (Figure 12b). These helium isotope ratios are much higher than found in typical MORBs, which normally fall in the range of 7–9 R_a. One would expect the helium isotopic signature in the hydrothermal fluids to agree with that in the volcanic rocks, since the vent fluid helium is extracted from the volcanic rocks or magma by hydrothermal circulation. *Lupton et al.* [2009] reported 17.8 R_a for one basalt sample collected from the summit of Lobster Caldera, while two additional samples on the flanks of Lobster reported previously by *Poreda and Craig* [1992] measured 21.9 and 22.1 R_a. Thus the helium end-member estimate of 18.7–19.3 R_a from the plume measurements at Lobster Caldera is in reasonable agreement with the basalt results.

[30] A similar fit for casts NLH-28, -29, -31, and -32 collected in the Central Caldera of the NWLSC gave $[^3\text{He}]/[^4\text{He}] = (1.47 \pm 0.055) \times 10^{-5}$, corresponding to $R/R_a = 10.6 \pm 0.4$ (Figure 12c).

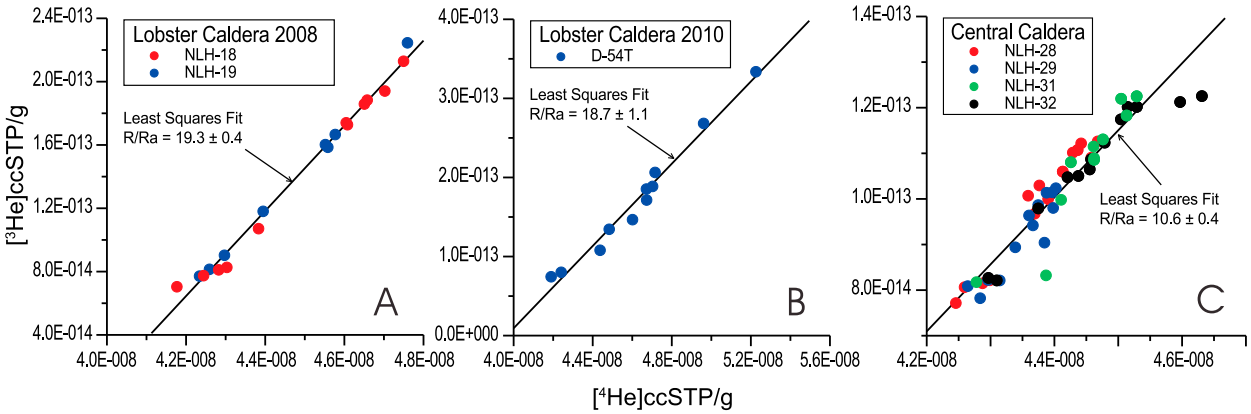

Figure 12. Plots of ^{3}He concentration versus ^{4}He concentration. (a) Lobster Caldera in 2008, (b) Lobster Caldera in 2010, and (c) for the Central Caldera on the NWLSC in 2008. Linear least squares fits give estimates of the end-member helium isotope ratio in units of R/R$_a$, where R = ^{3}He/^{4}He and R$_a$ = R$_{air}$ = 1.39 × 10^{-6}.

Lupton et al. [2009] measured ^{3}He/^{4}He ranging from 12.0 up to 20.8 R$_a$ for 14 rock samples from the NWLSC, and found 13.7, 15.6, and 15.9 R$_a$ in three basalts dredged from the Central Caldera volcanic edifice. Although this estimate for the end-member ^{3}He/^{4}He in the Central Caldera plume is lower than that measured in the volcanic rocks, the plume value of 10.6 R$_a$ is still elevated above typical MOR values. Overall, these results confirm that the mantle hot spot ^{3}He/^{4}He signature found in the volcanic rocks along the NWLSC-RR is also present in the hydrothermal fluids at Central Caldera and Lobster Caldera.

4. Summary and Conclusions

[31] A water column plume survey conducted in 2008 aboard the *R/V Southern Surveyor* detected several sites of active hydrothermal discharge along the Northwest Lau Spreading Center and the Rochambeau Rifts in the northern Lau Basin. The detection of hydrothermal plumes was based mainly on in situ suspended particle signals and measurements of excess ^{3}He/^{4}He and trace metals (TMn, TFe) in discrete bottle samples. Multibeam mapping shows that the NWLSC has a clearly defined axial high with two centers of enhanced magmatic output on the spreading axis, named Central Caldera and Southern Caldera. Hydrocasts into Southern Caldera and Central Caldera detected strong hydrothermal plume signals in δ^3He, TMn and suspended particles, showing that active hydrothermal vents exist at both of these sites. Although no strong plumes were detected in our two casts on the southern part of the NWLSC, three hydrocasts on the northern rift zone of the NWLSC all had excess δ^3He as well as suspended particles and TMn that varied in concert with the δ^3He. Overall these plume results indicate that at least two active hydrothermal sites exist along the ~55 km section of the NWLSC between 15.9°S and 15.5°S.

[32] In contrast to the NWLSC, multibeam mapping shows that the RR have no clear spreading axis. Instead, this extensional zone consists of a complex suite of pull-apart basins and volcanic centers extending from ~15.6°S up to 14.5°S. The southern part of the RR is dominated by Lobster Caldera, a large volcano with four separate rift zones radiating from the volcanic center. Hydrocasts into Lobster Caldera in 2008 detected high δ^3He (up to 239%), suspended particle and TMn signals, indicating active venting within the caldera. A repeat survey conducted in 2010 found even stronger plume signals in Lobster Caldera (δ^3He up to 359%), confirming that the site was still active two years later. Several additional hydrocasts within ~20 km of Lobster Caldera all show a clear δ^3He maximum (45–55%) at about 1500–1650 m depth. This δ^3He maximum is on a deeper isopycnal surface than the 1480 m deep water on the floor of Lobster Caldera, suggesting that a separate hydrothermal source is responsible for this regional plume.

[33] The elevated plume signals at Lobster Caldera and at Central Caldera allowed us to estimate certain characteristics of the pure end-member hydrothermal fluids generating the plumes at these two sites. The end-member ^{3}He/^{4}He ratios in the plumes at Lobster Caldera and Central Caldera (19 R$_a$ and 11 R$_a$, respectively) are elevated relative to typical MOR values, confirming that the hot spot or OIB-type signature found in the NWLSC-RR

volcanic rocks is also present in the hydrothermal fluids. The plumes at Lobster Caldera have low rise height, elevated Fe/Mn, and elevated ^{3}He/Mn, suggesting diffuse low-temperature venting rich in volatiles. After correcting for entrainment effects in the ascending plume, the correlation between ^{3}He concentration and temperature anomaly $\Delta\theta$ yielded an estimate of 2.1×10^{-17} mole/J for the end-member ^{3}He/heat ratio of the Lobster Caldera hydrothermal system. This value is elevated compared to steady state hydrothermal systems on mid-ocean ridges, suggesting that Lobster Caldera may have been recently perturbed by a magmatic input. In contrast to Lobster Caldera, the plumes at Central Caldera have high rise height, low Fe/Mn, and low ^{3}He/Mn, indicating the presence of high-temperature black smoker-type venting.

[34] The overall incidence of hydrothermal activity in the Northwest Lau Backarc Basin is quite high, as reflected by the background of δ^3He = 40% throughout the Basin. This background is much higher than typical values of δ^3He = 25% found at 2000–2500 m depth in southwestern Pacific waters [*Lupton et al.*, 2004], and is equivalent to background ^{3}He levels found along fast spreading segments of the MOR such as the southern EPR [*Urabe et al.*, 1995; *Lupton*, 1998]. The high level of hydrothermal activity throughout the northern Lau Basin is consistent with the high spreading rate (~100 mm/yr) for the NWLSC-RR and NELSC extensional zones.

[35] More specifically, this study has identified several localized sites of active hydrothermal discharge on the NWLSC – RR extensional zone, including Southern Caldera, Central Caldera, and Lobster Caldera. All three of these volcanic centers would make ideal targets for future studies involving submersible dives. Due to the unique mantle hot spot character of the Northwest Lau Backarc Basin, we speculate that the hydrothermal systems of the NWLSC-RR may be quite different from those found on typical MOR or backarc spreading centers.

Acknowledgments

[36] We thank the Australian Marine National Facility for granting us ship-time to conduct the SS07/2008 research voyage. The captain and crew of the *R/V Southern Surveyor* and scientific technical support staff rendered outstanding support during this voyage. We are grateful to the governments of Fiji and Tonga for their permission to conduct scientific research in their waters. We thank Tim McConachy and Bluewater Metals (South Pacific) Ltd. for collecting samples aboard the *Dorado Discovery* and for making the CTD data available. We thank Shannon Johns for drawing trace metal samples during voyage SS07, and Chris Yeats and the staff at CSIRO for archiving these samples and making them available to us. Susan Merle helped with the graphics. Dave Butterfield, Cornel de Ronde, and an anonymous reviewer provided constructive reviews of this paper. This work was support by the NOAA Vents Program. This is PMEL Contribution 3754.

References

Arculus, R. J. (2008), Voyage summary of SS07/2008 Northern Lau Vents Expedition, online report, Mar. Natl. Facil., Hobart, Tasmania, Australia. [Available at http://www.marine.csiro.au/nationalfacility/voyagedocs/2008/index.htm.]

Baker, E. T., J. E. Lupton, J. A. Resing, R. Baumberger, M. D. Lilley, S. L. Walker, and K. H. Rubin (2011), Unique event plumes from a 2008 eruption on the Northeast Lau Spreading Center, *Geochem. Geophys. Geosyst.*, *12*, Q0AF02, doi:10.1029/2011GC003725.

Bevis, M., et al. (1995), Geodetic observations of very rapid convergence and back-arc extension at the Tonga arc, *Nature*, *374*, 249–251, doi:10.1038/374249a0.

Bird, P. (2003), An updated digital model of plate boundaries, *Geochem. Geophys. Geosyst.*, *4*(3), 1027, doi:10.1029/2001GC000252.

Embley, R. W., et al. (2009), Extensive and diverse submarine volcanism and hydrothermal activity in the NE Lau Basin, *Eos Trans. AGU*, *90*(52), Abstract V51D-1719.

Farley, K. A., J. H. Natland, and H. Craig (1992), Binary mixing of enriched and undegassed (primitive?) mantle components (He, Sr, Nd, Pb) in Samoan lavas, *Earth Planet. Sci. Lett.*, *111*, 183–199, doi:10.1016/0012-821X(92)90178-X.

German, C. R., E. T. Baker, D. P. Connelly, J. E. Lupton, J. Resing, R. D. Prien, S. L. Walker, H. N. Edmonds, and C. H. Langmuir (2006), Hydrothermal exploration of the Fonualei Rift and Spreading Center and the Northeast Lau Spreading Center, *Geochem. Geophys. Geosyst.*, *7*, Q11022, doi:10.1029/2006GC001324.

Graham, D. W. (2002), Noble gas isotope geochemistry of mid-ocean ridge and ocean island basalts; characterization of mantle source reservoirs, in *Noble Gases in Geochemistry and Cosmochemistry*, edited by D. Porcelli, R. Wieler, and C. Ballentine, *Rev. Mineral. Geochem.*, *47*, 247–317, doi:10.2138/rmg.2002.47.8.

Hawkins, J. W. (1995), The geology of the Lau Basin, in *Back-arc Basins: Tectonics and Magmatism*, edited by B. Taylor, pp. 63–138, Plenum, New York.

Hilton, D. R., K. Hammerschmidt, G. Loock, and H. Friedrichsen (1993), Helium and argon isotope systematics of the central Lau Basin and Valu Fa Ridge: Evidence of crust/mantle interactions in a back-arc basin, *Geochim. Cosmochim. Acta*, *57*, 2819–2841, doi:10.1016/0016-7037(93)90392-A.

Honda, M., D. B. Patterson, I. McDougall, and T. J. Falloon (1993), Noble gases in submarine pillow basalt glasses from the Lau Basin: Detection of a solar component in backarc basin basalts, *Earth Planet. Sci. Lett.*, *120*, 135–148, doi:10.1016/0012-821X(93)90235-2.

Jackson, M. G., M. D. Kurz, S. R. Hart, and R. K. Workman (2007), New Samoan lavas from Ofu Island reveal a hemispherically heterogeneous high ^{3}He/^{4}He mantle, *Earth Planet. Sci. Lett.*, *264*, 360–374, doi:10.1016/j.epsl.2007.09.023.

Keller, N., R. J. Arculus, J. Hermann, and S. Richards (2008), Submarine back-arc lava with arc signature: Fonualei Spreading Center, northeast Lau Basin, Tonga, *J. Geophys. Res.*, *113*, B08S07, doi:10.1029/2007JB005451.

Kim, J., S. K. Son, J. W. Son, K. H. Kim, W. J. Shim, C. H. Kim, and K. Y. Lee (2009), Venting sites along the Fonualei and Northeast Lau spreading centers and evidence of hydrothermal activity at an off-axis caldera in the northeastern Lau Basin, *Geochem. J.*, *43*, 1–13, doi:10.2343/geochemj.0.0164.

Lavelle, J. W., E. T. Baker, and G. J. Massoth (1998), On the calculation of total heat, salt and tracer fluxes from ocean hydrothermal events, *Deep Sea Res., Part II*, *45*, 2619–2636, doi:10.1016/S0967-0645(98)00086-1.

Lupton, J. E. (1990), Water column hydrothermal plumes on the Juan de Fuca Ridge, *J. Geophys. Res.*, *95*, 12,829–12,842, doi:10.1029/JB095iB08p12829.

Lupton, J. E. (1998), Hydrothermal helium plumes in the Pacific Ocean, *J. Geophys. Res.*, *103*, 15,853–15,868, doi:10.1029/98JC00146.

Lupton, J. E., E. Baker, and G. Massoth (1989), Variable ^{3}He/heat ratios in submarine hydrothermal systems: Evidence from two plumes over the Juan de Fuca Ridge, *Nature*, *337*, 161–164, doi:10.1038/337161a0.

Lupton, J. E., E. T. Baker, M. J. Mottl, F. J. Sansone, C. G. Wheat, J. A. Resing, G. J. Massoth, C. I. Measures, and R. A. Feely (1993), Chemical and physical diversity of hydrothermal plumes along the East Pacific Rise, 8°45′N to 11°50′N, *Geophys. Res. Lett.*, *20*(24), 2913–2916, doi:10.1029/93GL00906.

Lupton, J. E., E. T. Baker, and G. J. Massoth (1999), Helium, heat, and the generation of hydrothermal event plumes on mid-ocean ridges, *Earth Planet. Sci. Lett.*, *171*, 343–350, doi:10.1016/S0012-821X(99)00149-1.

Lupton, J. E., D. G. Pyle, W. J. Jenkins, R. Greene, and L. Evans (2004), Evidence for an extensive hydrothermal plume in the Tonga-Fiji region of the south Pacific, *Geochem. Geophys. Geosyst.*, *5*, Q01003, doi:10.1029/2003GC000607.

Lupton, J. E., R. J. Arculus, R. R. Greene, L. J. Evans, and C. I. Goddard (2009), Helium isotope variations in seafloor basalts from the Northwest Lau Backarc Basin: Mapping the influence of the Samoan hotspot, *Geophys. Res. Lett.*, *36*, L17313, doi:10.1029/2009GL039468.

Lupton, J. E., J. A. Resing, E. T. Baker, R. W. Embley, G. J. Massoth, R. J. Arculus, R. R. Greene, J. H. Haxel, and N. J. Buck (2011), The regional hydrothermal helium-3 plume in the Tonga-Fiji-Samoa region of the south Pacific: An update, Abstract V51B-2518 presented at 2011 Fall Meeting, AGU, San Francisco, Calif., 5–9 Dec.

Martinez, F., and B. Taylor (2006), Modes of crustal accretion in back-arc basins: Inferences from the Lau Basin, in *Back-Arc Spreading Systems: Geological, Biological, Chemical, and Physical Interactions*, *Geophys. Monogr. Ser.*, vol. 166, edited by D. M. Christie et al., pp. 5–30, AGU, Washington, D. C., doi:10.1029/166GM03.

Massoth, G. J., E. T. Baker, J. E. Lupton, R. A. Feely, D. A. Butterfield, K. L. Von Damm, K. K. Roe, and G. T. Lebon (1994), Temporal and spatial variability of hydrothermal manganese and iron at Cleft Segment, Juan de Fuca Ridge, *J. Geophys. Res.*, *99*, 4905–4923, doi:10.1029/93JB02799.

McDougall, T. J. (1990), Bulk properties of "hot smoker" plumes, *Earth Planet. Sci. Lett.*, *99*, 185–194, doi:10.1016/0012-821X(90)90081-8.

McDuff, R. E. (1995), Physical dynamics of deep-sea hydrothermal plumes, in *Seafloor Hydrothermal Systems: Physical, Chemical, Biological, and Geological Interactions*, *Geophys. Monogr. Ser.*, vol. 91, edited by S. E. Humphris et al., pp. 357–368, AGU, Washington, D. C., doi:10.1029/GM091p0357.

Measures, C. I., J. Yuan, and J. A. Resing (1995), Determination of iron in seawater by flow injection analysis using in-line preconcentration and spectrophotometric detection, *Mar. Chem.*, *50*, 3–12, doi:10.1016/0304-4203(95)00022-J.

Natland, J. (1980), The progression of volcanism in the Samoan linear volcanic chain, *Am. J. Sci.*, *280*, 709–735.

Pelletier, B., S. Calmant, and R. Pillet (1998), Current tectonics of the Tonga-New Hebrides region, *Earth Planet. Sci. Lett.*, *164*, 263–276, doi:10.1016/S0012-821X(98)00212-X.

Pelletier, B., et al. (2001), Newly identified segments of the Pacific-Australia plate boundary along the North Fiji fransform zone, *Earth Planet. Sci. Lett.*, *193*, 347–358, doi:10.1016/S0012-821X(01)00522-2.

Poreda, R. J., and H. Craig (1992), He and Sr isotopes in the Lau Basin mantle: Depleted and primitive mantle components, *Earth Planet. Sci. Lett.*, *113*, 487–493, doi:10.1016/0012-821X(92)90126-G.

Resing, J. A., and M. J. Mottl (1992), Determination of manganese in seawater using flow injection analysis with on-line preconcentration and spectrophotometric detection, *Anal. Chem.*, *64*(22), 2682–2687, doi:10.1021/ac00046a006.

Resing, J. A., R. A. Feely, G. J. Massoth, and E. T. Baker (1999), The water-column chemical signature after the 1998 eruption of Axial Volcano, *Geophys. Res. Lett.*, *26*(24), 3645–3648, doi:10.1029/1999GL002350.

Resing, J. A., et al. (2011), An active submarine boninite eruption at West Mata Volcano in the NE Lau Basin, *Nat. Geosci.*, *4*, 799–806, doi:10.1038/ngeo1275.

Sedwick, P. N., G. M. McMurty, and J. D. MacDougall (1992), Chemistry of hydrothermal solutions from Pele's Vents, Loihi Seamount, Hawaii, *Geochim. Cosmochim. Acta*, *56*, 3643–3667, doi:10.1016/0016-7037(92)90159-G.

Turner, S., and C. Hawkesworth (1998), Using geochemistry to map mantle flow beneath the Lau Basin, *Geology*, *26*, 1019–1022, doi:10.1130/0091-7613(1998)026<1019:UGTMMF>2.3.CO;2.

Urabe, T., et al. (1995), The effect of magmatic activity on hydrothermal venting along the superfast-spreading East Pacific Rise, *Science*, *269*, 1092–1095, doi:10.1126/science.269.5227.1092.

Von Damm, K. L. (1995), Controls on the chemistry and temporal variability of seafloor hydrothermal fluids, in *Seafloor Hydrothermal Systems: Physical, Chemical, Biological, and Geological Interactions*, *Geophys. Monogr. Ser.*, vol. 91, edited by S. E. Humphris et al., pp. 222–247, AGU, Washington, D. C., doi:10.1029/GM091p0222.

Wiens, D. A., K. A. Kelley, and T. Plank (2006), Mantle temperature variations beneath back-arc spreading centers inferred from seismology, petrology, and bathymetry, *Earth Planet. Sci. Lett.*, *248*, 30–42, doi:10.1016/j.epsl.2006.04.011.

Young, C., and J. E. Lupton (1983), An ultratight fluid sampling system using cold-welded copper tubing, *Eos Trans. AGU*, *64*, 735.

Zellmer, K. E., and B. Taylor (2001), A three-plate kinematic model for Lau Basin opening, *Geochem. Geophys. Geosyst.*, *2*(5), 1020, doi:10.1029/2000GC000106.